SUPPLEMENTARY FIGURES

Nagpal *et al*

The zinc finger of DNA Ligase 3α binds to nucleosomes via an arginine anchor

Table S1. The concentration in each batch of the extracts calculated in flow-cell of c-trap and measured using the calibration curve from Fig S1.

EXTRACT		Dilution used in C-Trap	XRCC1-YFP nM in flow cell	Halo-Lig3α nM in flow cell
Halo-635-Lig3α- XRCC1-YFP	BATCH1	1:10	0.7	0.2
	BATCH2	1:10	1.3	0.11
	BATCH3	1:10	1.4	0.11
	BATCH4	1:10	0.24	0.16
	BATCH5	1:10	0.6	0.28
	BATCH6	1:10	0.5	0.34
	BATCH7	1:10	1.2	0.17
	ZnF-BRCT	1:10	1.24	0.83
	ZnF DEL	1:10	0.12	0.15
Halo-Lig3K421A- XRCC1-YFP	BATCH1	1:10	0.35	0.17
Halo-Lig3K421A- XRCC1-YFP	BATCH 2	1:10	0.62	0.23

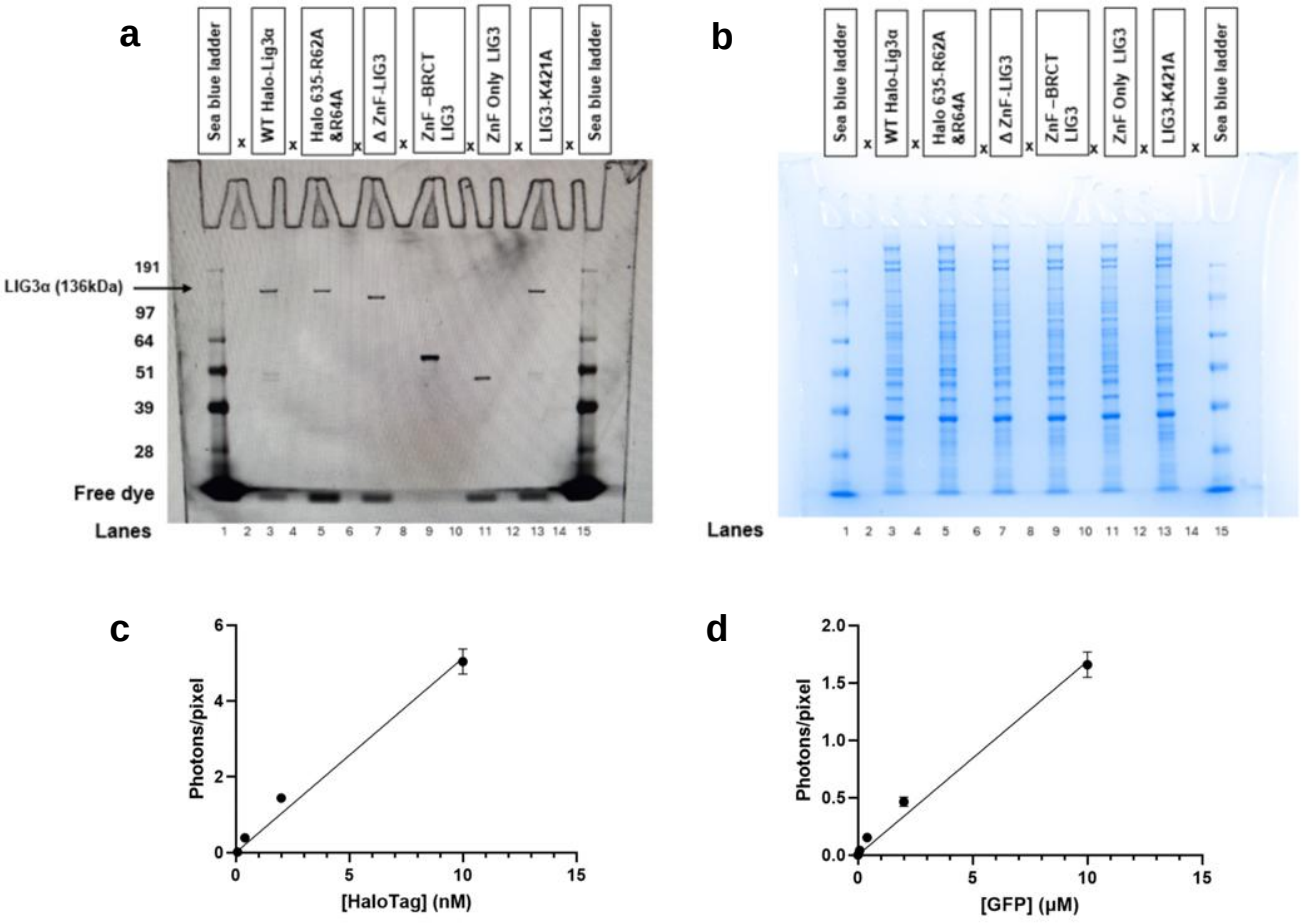

Fig. S1: Characterization of expressed proteins in our extract : (a) SDS-PAGE analysis of all Halo Tag-LIG3α variants used for the study. **(b)** Since Halo Tag dye (JF-635) crosslinks to the protein after labelling, Halo Tag fluorescence was directly imaged after running the denaturation gel, Coomassie blue gel staining. **(c)** Standard curves collected on purified Halo-Tag protein conjugated to JF-635 **(D)** GFP standard with a linear fit (these curves have been adapted from SMADNE paper https://doi.org/10.1093/nar/gkad095 Supplement fig1). In support of Figure 1.

Fig. S1

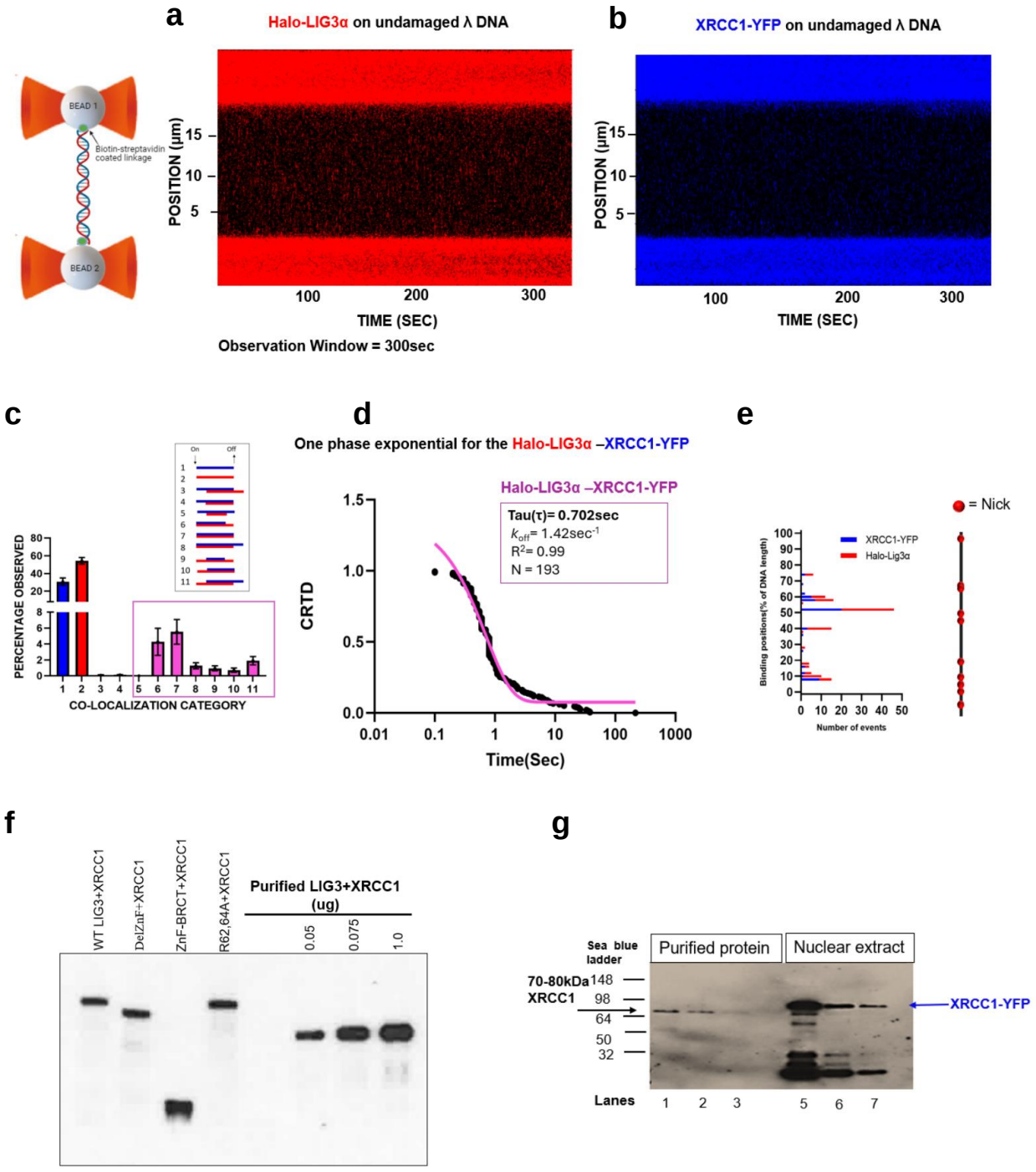

Fig. S2: SMADNE analysis of Halo 635-LIG3α-XRCC1-YFP binding to an un-damaged λ DNA substrate. **(a)** Representative five-minute kymograph of Halo-635-LIG3α on an un-damaged λDNA. There were no events observed during this window at 10pN tension. **(b)** Representative five-minute kymograph of XRCC1-YFP on an un-damaged λDNA. There were no events observed during this window at 10pN tension (note: both the kymographs are taking from the same window just the laser color is adjusted according to the frequency of fluoro-dye tags. **(c)** The distribution of the 11 categories for Halo 635-LIG3α and XRCC1-YFP binding nicked λ DNA. Error bars represent the SEM of fourteen experiments. **(d)** Cumulative residence time distribution (CRTD) for a set of (N=193) co-localized binding evets of Halo 635-LIG3α-XRCC1-YFP on the nicked λ DNA, with a single exponential fit shown in pink. **(e)** Binding positional analysis of Halo 635-LIG3α-XRCC1-YFP shown at the expected sites, that were bound multiple times to the nicked λ DNA digested with nicking enzyme Nt.BspQ1 generating eight observable ligatable nicks. **(f)** Western blots for extracts with LIG3α variants and the WT-LIG3αon the left and purified LIG3α-XRCC1 on the right lanes. (**h)** Western blots for extracts overexpressing XRCC1-YFP , with bands corresponding to endogenous XRCC1 in 3, 1.5, 0.75 μL nuclear extract lane. Purified XRCC1 was loaded in initial 1-3 lanes. In support of Figure 1.

Fig. S2

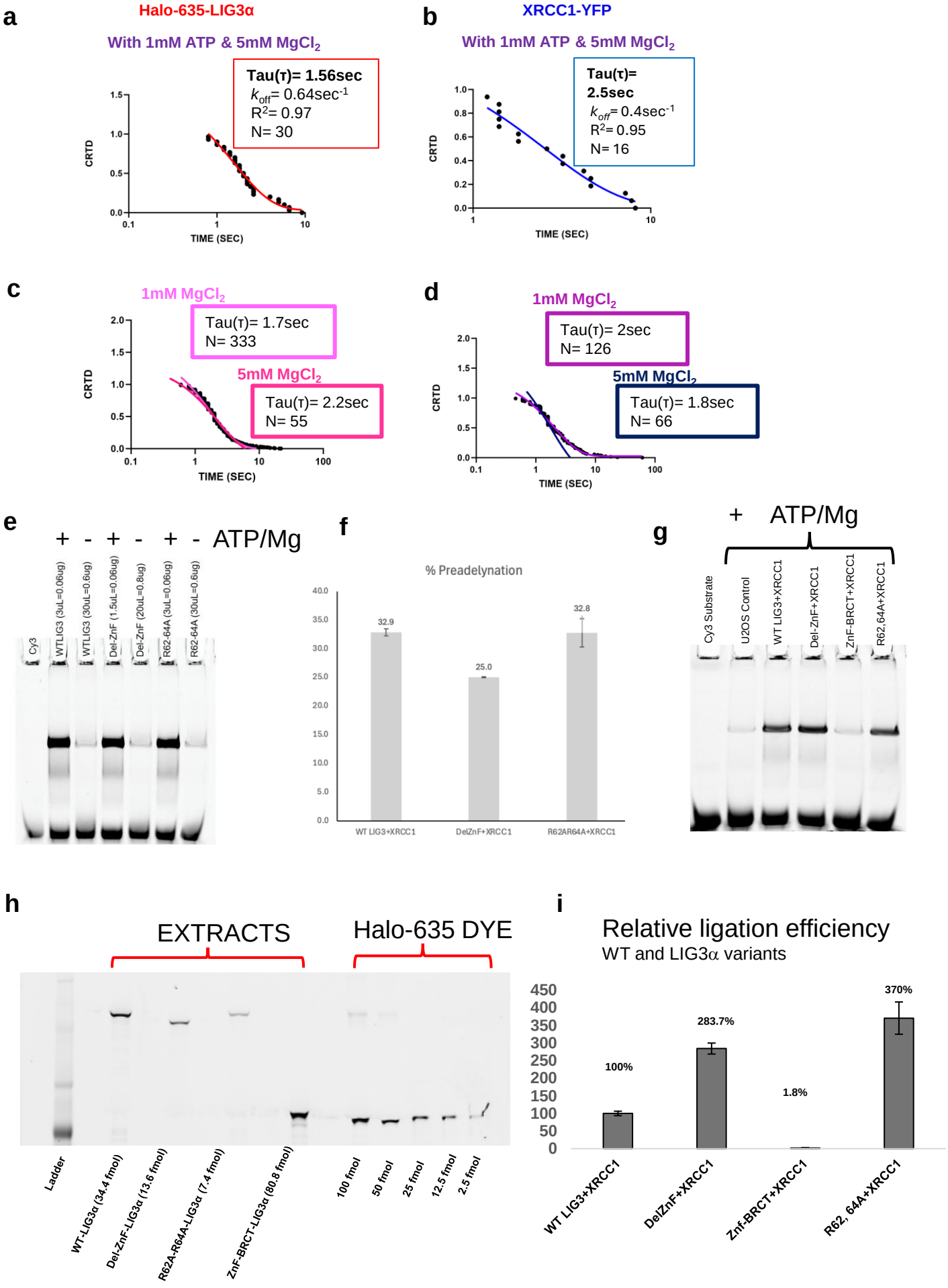

Fig. S3

See next page for figure legend

Fig. S3 **(a)** Cumulative residence time distribution (CRTD) for Halo-635-LIG3α in presence of 1mM ATP and 5mM $MgCl_2$. **(b)** Cumulative residence time distribution (CRTD) for XRCC1-YFP in presence of 1mM ATP and 5mM $MgCl_2$. **(c)** Cumulative residence time distribution (CRTD) for Halo-635-LIG3α in presence of 1mM (pink) or 5 mM $MgCl_2$ (red). **(d)** Cumulative residence time distribution (CRTD) for XRCC1-YFP in presence of 1mM $MgCl_2$ (purple) and 5mM (blue). **(e)** Ligation assay in all the variants of LIG3α used in nuclear extracts in absence or presence of 1 mM ATP and 10 mM $MgCl_2$. **(f)** Based on the absence of ATP/$MgCl_2$ lanes, the amount of preadelynated LIG3 in nuclear extracts. (**g**) Relative ligation efficiencies from nuclear extracts fractions in the presence of 1 mM ATP and 10 mM $MgCl_2$. (**h**) SDS gel showing relative protein concentrations. (**i**) Ligation efficiency of WT and LIG3α variants corrected for relative protein concentrations and background ligase activity in our nuclear extracts. In support of Figure 2.

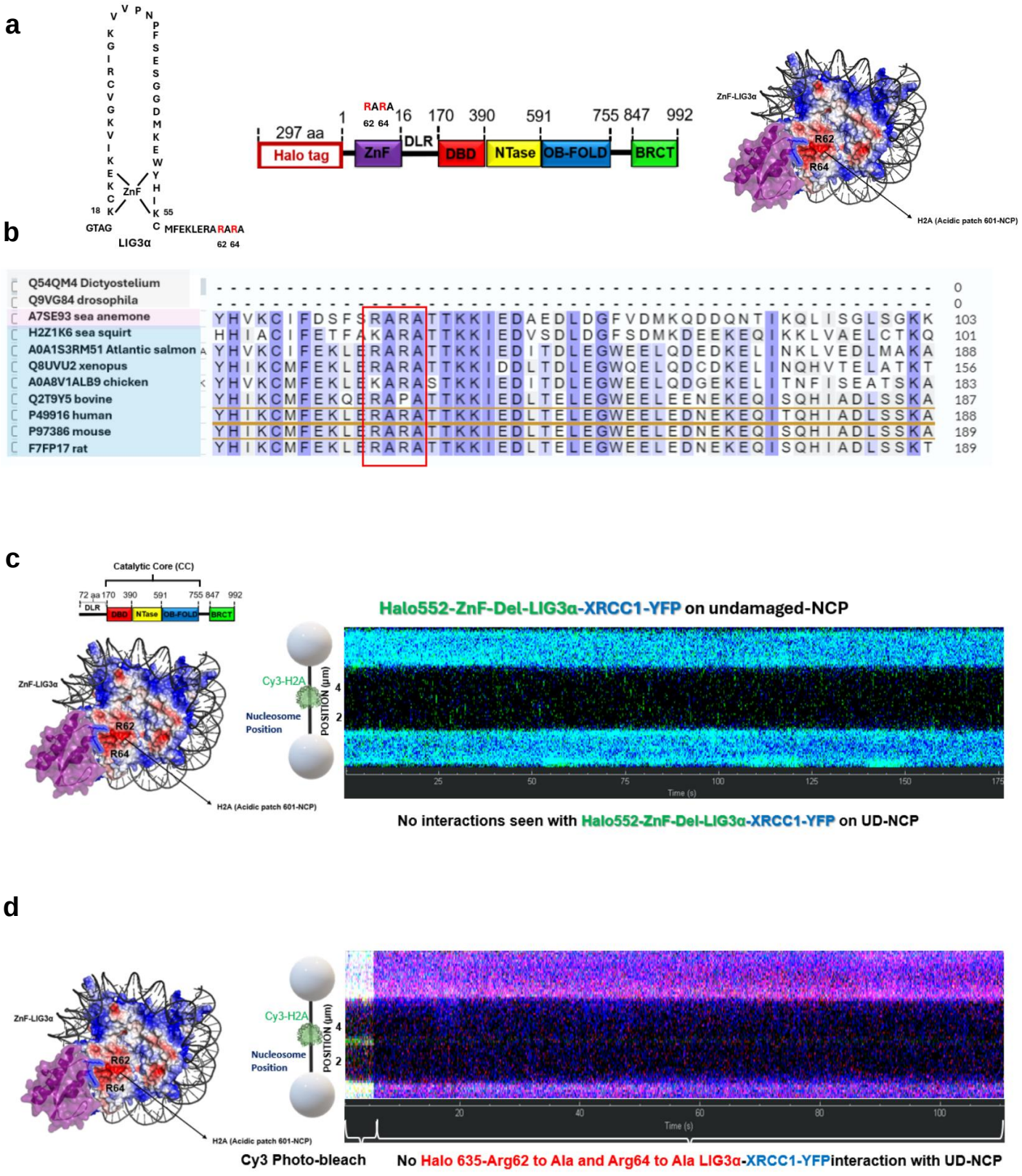

Fig. S4: **(a)** A representative model design of the ZnF domain of LIG3α showing the position of Arg anchor. **(b)** Sequence alignment showing the Arg anchor as "RARA" which is conserved in many species. **(c)** Representative kymograph of del-ZnF variant of Halo-635-LIG3α on an un-damaged λDNA. **(d)** Representative kymograph of del-ZnF variant of Halo-635-LIG3α on an un-damaged λDNA. In support of Figure 5.

Fig. S4

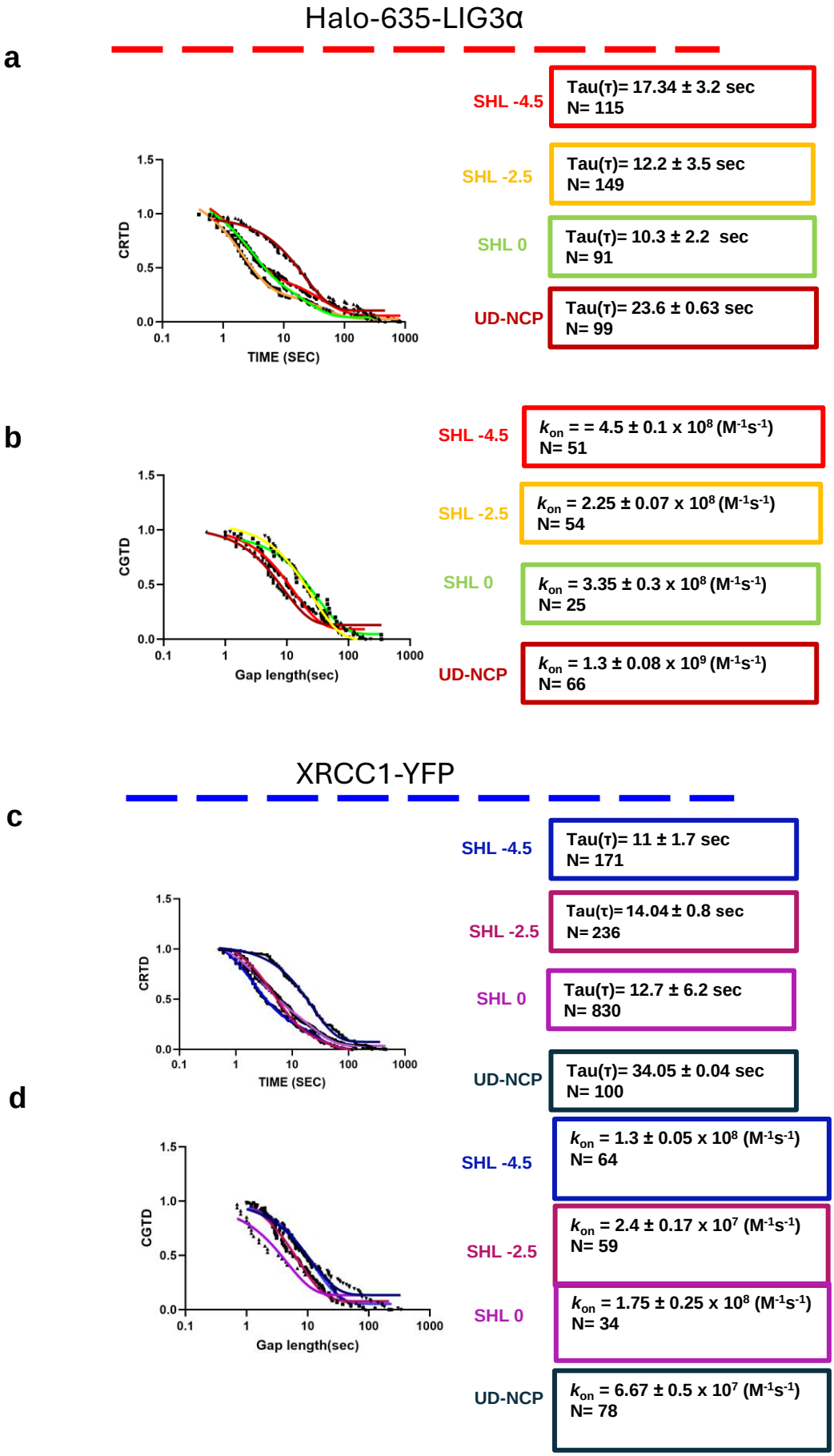

Fig. S5: Combined CRTD/CGTD plots of LIG3α-XRCC1 (a,b) Comparative combined CRTD & CGTD plots for LIG3α binding to SHL-4.5, SHL-2.5, SHL0 & UD-NCP. **(c,d)** Comparative combined CRTD & CGTD plots for XRCC1 binding to SHL-4.5, SHL-2.5, SHL0 & UD-NCP. In support of Figure 6.

Fig. S5

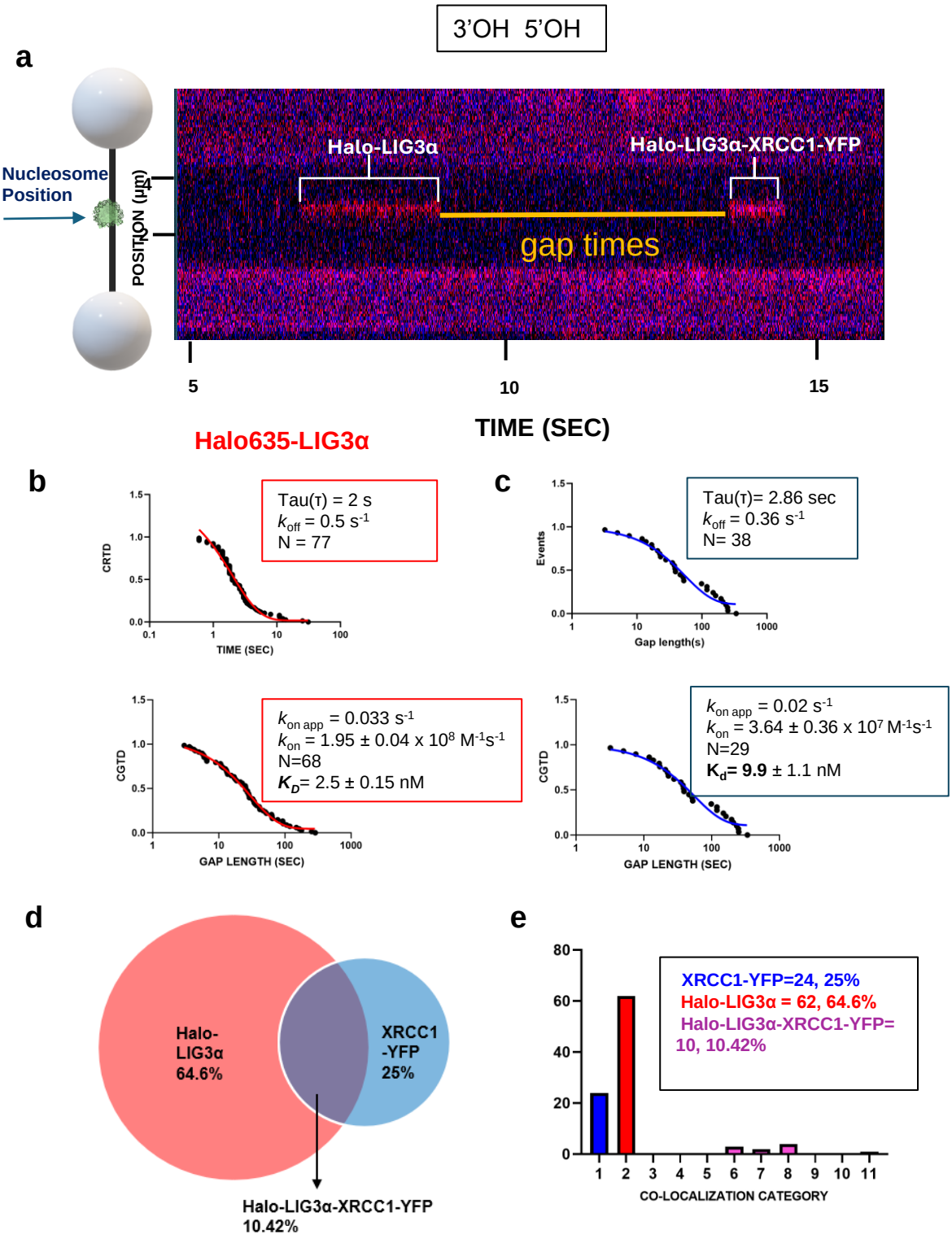

Fig. S6: Binding kinetics of Halo 635-LIG3α-XRCC1-YFP to one non-ligatable nick substrate. (a) A corresponding kymograph of an observation for Halo 635-LIG3α-XRCC1-YFP binding to a non-ligatable nick λ DNA. **(b)** Cumulative residence time distribution (CRTD) and cumulative gap time distribution (CGTD), analysis for Halo 635-LIG3α binding a non-ligatable nick, with a single exponential fit shown in red. **(c)** Cumulative residence time distribution (CRTD) and cumulative gap time distribution (CGTD), analysis for XRCC1-YFP binding, a non-ligatable nick with a single exponential fit shown in blue. **(d)** Percentage of events that were Halo 635-LIG3α alone in red and XRCC1-YFP alone in blue, or colocalized together in the middle as pink. **(e)** The distribution of the 11 categories for Halo 635-LIG3α and XRCC1-YFP binding to a non-ligatable nick. Error bars represent the SEM of two experiments. In support of Figure 6.

Fig. S6